Published in final edited form as:
Nanomedicine (Lond). 2014 August ; 9(11): 1595–1612. doi:10.2217/nnm.13.136.

Comparative biophysical properties of tenofovir-loaded, thiolated and nonthiolated chitosan nanoparticles intended for HIV prevention

Jianing Meng, **Tao Zhang**, **Vivek Agrahari**, **Miezan J Ezoulin**, and **Bi-Botti C Youan***
Laboratory of Future Nanomedicines & Theoretical Chronopharmaceutics, Division of Pharmaceutical Sciences, University of Missouri, Kansas City, MO 64108, USA

Abstract

Aim—This study is designed to test the hypothesis that tenofovir-loaded (an anti-HIV microbicide) chitosan–thioglycolic acid-conjugated (CS–TGA) nanoparticles (NPs) exhibit superior biophysical properties for mucoadhesion compared with those of native CS NPs.

Materials & methods—The NPs are prepared by ionotropic gelation. The particle mean diameter, encapsulation efficiency and release profile are analyzed by dynamic light scattering and UV spectroscopy, respectively. The cytotoxicity, cellular uptake and uptake mechanism are assessed on VK2/E6E7 and End1/E6E7 cell lines by colorimetry/fluorimetry, and percentage mucoadhesion is assessed using porcine vaginal tissue.

Results—The mean diameter of the optimal NP formulations ranges from 240 to 252 nm, with a maximal encapsulation efficiency of 22.60%. Tenofovir release from CS and CS–TGA NPs follows first-order and Higuchi models, respectively. Both NPs are noncytotoxic in 48 h. The cellular uptake, which is time dependent, mainly occurs via the caveolin-mediated pathway. The percentage of mucoadhesion of CS–TGA NPs is fivefold higher than that of CS NPs, and reached up to 65% after 2 h.

Conclusion—Collectively, CS–TGA NPs exhibit superior biophysical properties and can potentially maximize the retention time of a topical microbicide, such as tenofovir, intended for the prevention of HIV transmission.

*Author for correspondence: Tel.: +1 816 235 2410, Fax: +1 816 235 5779, youanb@umkc.edu.

Disclaimer
The content is solely the responsibility of the authors and does not necessarily represent the official view of the National Institute of Allergy and Infectious Diseases or the National Institute of Health.

Financial & competing interests disclosure
The work presented was supported by Grant Number R01A1087304 from the National Institute of Allergy and Infectious Diseases (MD, USA). The authors are grateful to VM Dusevich (School of Dentistry, University of Missouri, USA) for the transmission electron microscopy images. The authors would also like to thank C Forster (Fairview Farm Meat Co., KS, USA) for kindly providing the fresh porcine vaginal tissue. The authors have no other relevant affiliations or financial involvement with any organization or entity with a financial interest in or financial conflict with the subject matter or materials discussed in the manuscript apart from those disclosed.
No writing assistance was utilized in the production of this manuscript.

Keywords

HIV prevention; mucoadhesion; tenofovir; thiolated chitosan; nanoparticle; vaginal drug delivery

HIV/AIDS has caused more than 25 million deaths since it was first discovered, making it one of the most destructive epidemics recorded in history [1]. Nowadays, HIV infection rates have reached pandemic levels worldwide, with the number of people living with HIV in 2012 estimated at 35.3 million [2]. Among these, women represent a growing proportion, and the ratio of infected men to women is particularly skewed among young people [3]. Women are more susceptible to infection than men due not only to human physiology but also social, economic and legal disadvantages, which limit their ability to protect themselves, especially in Asia and Africa [3]. In sub-Saharan Africa, for every HIV-infected young man (15–24 years old) there are nearly three infected young women [4]. Therefore, there is an urgent and critical need to identify effective strategies that can reduce women's risk of HIV and other sexually transmitted infections.

More than 80% of HIV infections in women occur through sexual contact with an infected partner [5]. While unprotected heterosexual vaginal intercourse has become a predominant route of infection for this disease, several studies have shown that the vagina is also a suitable site for the delivery of drugs [6]. The large surface area, permeability and rich blood supply of the mucous membrane of the vagina provide significant potential for the delivery of drugs [7]. Polymer-based nanoparticles (NPs) have been considered in the intravaginal delivery of microbicides as they could avoid the degradation, improve the uptake and allow the sustained release of drugs [8]. Various NPs of this type have been developed, such as the poly(lactic-*co*-glycolic) acid NPs [9] and solid lipid NPs [10]. Recent advances have been made in the area of bioadhesive NPs, which show great promise for use as controlled, intravaginal delivery systems. By prolonging the contact time of the microbicide with the vaginal tissue, the effect of the microbicide could be significantly improved. These improvements range from better treatment of local pathologies to superior drug bioavailability and controlled release to enhance patient compliance [11].

Numerous polymers and hydrogels have been used to prolong the residence time at the site of application. Among these, chitosan (CS) is a promising candidate due to its favorable biological properties, such as nontoxicity, biocompatibility and biodegradability [12]. Compared with unmodified CS, it has been shown that the thiolation of CS, by the covalent attachment of thioglycolic acid (TGA), leads to a significantly improved mucoadhesion [13]. CS–thioglycolic acid conjugation (CS–TGA) displays thiol-bearing side chains that mimic the natural mechanism of secreted mucus glycoproteins [14]. Based on thiol/disulfide exchange reactions and/or a simple oxidation process, disulfide bonds are formed between polymers and cysteine-rich subdomains of mucus glycoproteins so that the polymers can covalently anchor to the mucus layer [15].

We have recently engineered tenofovir (TFV)-loaded CS NPs to increase drug retention in the topical route [16]. In order to further maximize microbicide mucoadhesion, CS–TGA is used instead of native CS during the preparation of NPs. This study is thus designed to test the hypothesis that anti-HIV microbicide (TFV)-loaded CS–TGA NPs exhibit superior

biophysical properties for mucoadhesion to the vaginal epithelium compared with those of native CS NPs and gel formulations. TFV, chosen as a model drug, is a nucleotide analog reverse-transcriptase inhibitor. TFV has been widely applied in HIV-1 therapy due to its activity against a range of HIV-1 subtypes. It inhibits enzyme activity by attaching to its active site, subsequently disabling the binding of the natural substrate deoxyadenosine 5′-triphosphate. Once TFV is inserted into the viral DNA synthesis steps, the normal 5′ to 3′ links are prevented from occurring, resulting in HIV DNA chain termination [17]. CS–TGA is chosen as a matrix of the drug carrier, and sodium tripolyphosphate (TPP) works as a crosslinking agent. NPs are prepared on the basis of the ionic gelation of CS–TGA with TPP anions [18].

Materials & methods

Preparation of TFV-loaded CS–TGA-based NPs

The method of preparation is adapted from the method described by Fernandez-Urrusuno *et al.* [19] and provided in the Supplementary information (see online at: www.futuremedicine.com/doi/suppl/10.2217/NNM.13.136). The concentrations of the CS–TGA, TPP and TFV solutions are shown in Supplementary Figure S1. The preparation of fluorescein isothiocyanate (FITC)-labeled CS and CS–TGA is based on the reaction between the isothiocyanate groups of FITC and the amino groups of CS [20], as previously described [21].

Determination of drug-encapsulation efficiency

After centrifugation, the supernatant is analyzed to determine the percentage drug encapsulation efficiency (EE%; Supplementary information). The EE% of TFV is calculated using Equation 1:

$$EE(\%)=\frac{Total\ amount\ of\ TFV-Free\ TFV}{Total\ amount\ of\ TFV}\times 100 \quad \text{(Equation 1)}$$

Size & size distribution analysis

The particle mean diameter and polydispersity index in water medium are determined by dynamic light scattering (Supplementary information) [22]. The polydispersity index is given in Equation 2:

$$PDI=\frac{K_2}{K_1{}^2} \quad \text{(Equation 2)}$$

where K_1 is an effective mean diffusion coefficient K_2 and is the relative width of the size distribution if normalized K_1 by [22]. A sample with a polydispersity index of <0.05 is considered monodispersed according to the National Institute Standard [1].

Morphological analysis

The morphology of the NPs is examined by scanning electron microscopy and transmission electron microscopy (Supplementary information).

In vitro TFV release profile

The *in vitro* release of NPs is compared with a hydroxyethyl cellulose (HEC) gel containing TFV, with TFV powder used as a control (Supplementary information). The vaginal fluid stimulant is prepared according to previous reports [23]. One-hundred percent drug release is obtained from complete enzymatic digestion of NPs using lysozyme after 120 h using the method of Don *et al.* [24]. The drug-release data are fitted into the kinetic models below (Equations 3–5) related to zero-order, first-order, and Higuchi models, respectively, to elucidate the underlying mechanisms [25].

For zero-order kinetics:

$$Q = k_0 t \quad \text{(Equation 3)}$$

where Q represents the percentage of the drug released in time t and k_0 is the apparent release rate constant, or zero-order release constant.

For first-order kinetics:

$$ln(1-Q) = -k_1 t \quad \text{(Equation 4)}$$

where Q represents the percentage of the drug released in time t and k_1 is the first-order release constant.

For Higuchi model:

$$Q = k_H t^{1/2} \quad \text{(Equation 5)}$$

where Q represents the percentage of the drug released in time t and k_H is the Higuchi dissolution constant.

Cell cultures

Two cell lines are used in this study: VK2/E6E7 and End1/E6E7 (Supplementary information).

Cytotoxicity studies

To measure lactate dehydrogenase (LDH) release, cells are seeded in a 96-well plate (Supplementary information). After 80% confluence is reached, the cells are incubated with 100 µl of media containing 1 mg/ml blank or TFV-loaded CS or CS–TGA NPs (see characteristics in Table 1), or 200 µg/ml TFV in each well. The percentage of LDH released by the cell membrane is calculated using Equation 6:

$$LDH\ release\ (\%) = \frac{F_{Experimental} - F_{Background}}{F_{Positive} - F_{Background}} \times 100 \quad \text{(Equation 6)}$$

where $F_{Experimental}$, $F_{Background}$ and $F_{Positive}$ represent the fluorescence intensity of NP-treated, background (without cells) and positive control (cells treated with 1% Triton™ X-100; Sigma-Aldrich, MO, USA) wells, respectively.

The cell viability is determined by adding 3-(4,5-dimethylthiazol-2-yl)-5-(3-carboxymethoxyphenyl)-2-(4-sulfophenyl)-2H-tetrazolium, inner salt (MTS) and then checking the amount of a colored formazan product that was bioreduced from MTS by the cells (Supplementary information). The cell viability is expressed using Equation 7:

$$Viability\,(\%) = \frac{A_{Test}}{A_{Control}} \times 100 \quad \text{(Equation 7)}$$

where A_{Test} and $A_{Control}$ represent the absorbance related to the amount of formazan detected in viable cells in wells treated with NPs and not treated with NPs, respectively.

The *Lactobacillus* viability assay is performed in order to assess the effect of CS NPs on *Lactobacillus crispatus* growth using the established method [26]. Briefly, the bacteria density is adjusted to an optical density of 0.06 at 670 nm, corresponding to a 0.5 McFarland standard or 10^8 colony forming units/ml [27]. The percent viability is calculated using Equation 7.

Cellular uptake studies

Cellular uptake studies are performed using a microplate reader and a confocal microscope, as previously described [28] and as described in the Supplementary information. The cellular uptake efficiency is calculated using Equation 8:

$$Cellular\ uptake\,(\%) = \frac{F_{Cell}}{F_{Control}} \times 100 \quad \text{(Equation 8)}$$

where F_{Cell} and $F_{Control}$ represent the fluorescence intensity related to the amount of particles taken up in the cells in test wells and in the control wells, respectively.

Flow cytometry analysis

Both VK2/E6E7 and End1/E6E7 cell lines are cultured in T-25 culture flasks (Sigma-Aldrich) until 80% confluence is reached. FITC-labeled CS and CS–TGA NPs (500 μg/ml) are incubated with cells for 48 h (Supplementary information).

Assessment of uptake using fluorescence microscopy

Both VK2/E6E7 and End1/E6E7 cells are seeded on the 96-well plate at a concentration of 2×10^5 cells/ml and incubated at room temperature for 20 min (Supplementary information) [29].

Cellular uptake mechanism study

In all cases, the treatment of the cells with CS and CS–TGA NPs is carried out in the presence of the respective NPs at the same concentration as used for the pretreatment. Following treatment under these various conditions, the cells are harvested after 24 h and analyzed as described above (Supplementary information) [30].

Mucoadhesion study

The bioadhesive properties of the NPs are determined as described by Ranga Rao and Buri, and Albrecht *et al.* (Supplementary information) [31,32], for the comparison of CS and CS–TGA NPs using the infusion and immersion method [33]. The percent mucoadhesion (MA %) is calculated using Equation 9:

$$MA\,(\%) = \frac{F_{Initial} - F}{F_{Initial}} \quad \text{(Equation 9)}$$

where $F_{Initial}$ represents the initial fluorescence and F represents the fluorescence after the treatment [34]. The skin sections (5 mm) are mounted on glass slides and visualized through a fluorescence microscope without any additional staining or treatment [35].

Statistical data analysis

The study is designed according to the Box–Behnken experimental design method [36]. The polynomial equations relating the independent variables to dependent variables are obtained by Box–Behnken design software (JMP8; SAS Institute Inc., NC, USA), which is used for response optimization. The results are expressed as the mean of at least three experiments ± the standard error of the mean. Statistical data analysis is performed using the Student's *t*-test; two tails with 95% CI ($p < 0.05$) are used as the minimal level of significance.

Results & discussion

Formulation & characterization of CS–TGA NPs

The Box–Behnken design utilized in this study has several advantages. It requires less runs in comparison with other experimental designs. Three factors are chosen as independent variables: X_1 = concentration of CS–TGA (w/v%); X_2 = TPP/CS–TGA weight ratio; and X_3 = drug/CS–TGA weight ratio. Each factor is studied at three levels, represented by −1, 0 and 1. Two dependent variables (Y_1 = EE%; and Y_2 = particle mean diameter [nm]), are chosen as responses. It is also able to avoid extreme conditions, as it does not contain combinations where all of the factors are at their highest or lowest levels [37]. Figure 1A shows the actual EE% against the predicted EE% with a regression line and 95% confidence curves. The horizontal line is the sample mean. The regression line and the 95% confidence curves cross the sample mean, which means that the actual EE% correlates with the predicted EE%; the factors in this model explain a significant proportion of the variation in the EE%. According to the acceptability criteria for the nanoencapsulation process, a p-value of <0.1 and a coefficient of determination (r^2) value of >0.9 is required. Since the polynomial equations for Y_1 fit well ($p = 0.0012$; $r^2 = 0.98 > 0.90$) (Figure 1A) [25], it can be used for Y_1 response optimization purposes. The polynomial Equation 10 below expresses the influence of the independent variables on Y_1 (EE%):

$$Y_1 = 5.14 + 2.87X_1 + 3.10X_2 - 3.40X_3 + 2.80X_1X_2 - 1.97X_1X_3 - 1.88X_2X_3 + 3.10{X_1}^2 - 1.03{X_2}^2 - 2.78{X_3}^2 \quad \text{(Equation 10)}$$

A Pareto chart is constructed in Figure 1B to visualize the significance of the variables in Equation 10. The values indicated on the bars of the Pareto chart represent the standardized effects, which are the t-values calculated based on Equation 11:

$$t=\frac{|E_X|}{SE_e} \quad \text{(Equation 11)}$$

where E_X is the estimate of the factor effect, which is the coefficient in Equation 10, and SE_e is the standard error of the factor effect [38]. The obtained *t*, which indicates the main effect of the independent variables and interactions on the Y_1 value, is compared with a tabulated critical t-value (the absolute value of $t_{Critical} = 2.57$) at $p < 0.05$, which is determined at $\alpha = 0.05$ for the residual degrees of freedom (df), where df = 5 [39]; both $t_{Critical}$ values are shown in the two vertical lines in Figure 1B. The factors whose length passed the vertical line indicate significance on the response value [40]. The positive sign of the coefficient shows a positive effect on the size of the responses, while the negative signs indicate a negative effect.

According to Figure 1B, X_1, X_2, X_3, X_1*X_1, X_1*X_2, X_3*X_3, X_1*X_3 and X_2*X_3 all contribute substantially to the EE%. CS–TGA is used in this study as a polymeric matrix; the encapsulation of the drug is based on the interaction between the amino groups of CS–TGA and the phosphate groups of the drug. Higher CS concentrations (X_1) mean more total available amino groups in CS molecules, and more drug molecules could interact with CS–TGA through electrostatic forces. Therefore, the EE% increases with increasing X_1, and X_1*X_1 influences the EE% positively based on the same reason. From Figures 1B & 1C, the concentration of CS (X_1) has a curvilinear effect on the EE%. Below the coded value of −1, the EE% begins to increase. It may be due to the decreased viscosity effect at a lower concentration. It has already been reported that low viscosity associated with decreased CS concentration allows the drug to move around the polymer chain, and consequently improves its entrapment [41]. TPP works as the crosslinking agent; many more polymer molecules could be linked together and form NPs while increasing the ratio of TPP/CS (X_2). The EE% increased with the TPP/CS–TGA (w/w) (X_2) linearly. Since both CS and TPP strengthen the mass and crosslink density of the polymeric matrix, the combination of X_1*X_1 and X_1*X_2 also demonstrates a positive effect on EE%. An increase of drug/CS–TGA (w/w) X_3 has a decreasing effect on the EE%. The higher the relative amount of drug to polymer in the solution (X_3) the lower the EE%, because fewer polymers would be available for drug encapsulation. Therefore, the combination of X_1*X_3 and X_2*X_3 demonstrates a negative effect on the EE% (Y_1). It also appears that the EE% (Y_1) correlated curvilinearly with X_3. The drug/CS–TGA ratio (X_3) appears to increase the EE%. A possible reason is that the aqueous solution of TFV is a weak acid with two pKa values at 3.8 and 6.7 [42]. At high concentration, it is possible that TFV influences the pH of the solvent, which is conducive to the ionization of CS or CS–TGA. The subsequent water solubilization is needed for effective crosslinking with TPP [41]. However, this effect is limited by TFV's high water solubility (1.87 mg/ml in water) [43]. In Figure 1C, it is evident that a higher level of X_1 and X_2 and a lower level of X_3 favored higher EE% (Y_1). Supplementary Figure S2 shows the results from the analysis of variance. Based on Equation 10, and the interaction plot shown in Figure 1, the optimal formulation that

exhibited the highest EE% (25.78 ± 3.77%) is selected: X_1, X_2 and X_3 are 1, 0.96 and −1, respectively.

To confirm the analysis, a checkpoint analysis is performed. Two random points out of the 15 runs of the experiment ($X_1 = -0.5$, $X_2 = -0.5$ and $X_3 = -0.5$, and $X_1 = 0.5$, $X_2 = 0.5$ and $X_3 = 0.5$) and the theoretically optimum point resulting from the statistical model (with the three factors set at $X_1 = 1$, $X_2 = 0.96$ and $X_3 = -1$) are selected. As shown in Table 2, the EE % of the tested points are close to the predicted values. The differences between the measured and predicted values are not found to be statistically significant ($p > 0.05$). According to the Student's *t*-test, the t-value of the optimal point (C3) is 3.00 (df = 2; $\alpha = 0.05$; the absolute value of $t_{Critical} = 4.30$), which indicates that the optimal EE% (22.60%) obtained from the experiment appeared to be close to the prediction (25.78%) derived from the model. The other two checkpoints (C1 and C2) lead to similar responses (t-values are 0.90 and 0.72, respectively). Therefore, it can be reasonably concluded that, under these checkpoint conditions, the model fits the data satisfactorily and is valid for predicting the EE %. The model prediction equation is an acceptable tool to predict the EE% of NPs in this study. The NP samples used for all of the assays below are prepared under optimal conditions.

However, the r^2 of the polynomial equation for particle mean diameterY_2 (0.67) is below the threshold for acceptability (0.70) [25]. One possible reason for this is the presence of the thiol groups on CS–TGA chains. It is noteworthy that the molecular weight of CS–TGA (10–150 kDa) is relatively lower than that of CS (50–190 kDa). The size of CS-based particles is found to be proportional to the macromolecules' molecular weight (data not shown). By contrast, there is no statistically significant difference in the particle mean diameters of CS NPs (240.1 nm) and CS–TGA NPs (252.3 nm) (Table 1). Therefore, it is reasonable to infer that initially the CS–TGA tends to form small NPs. However, the superfluous thiol groups have a strong tendency to form inter- and intra-molecular disulfide bonds with each other. These thiol groups provide a cohesive force to link the small fragments to form larger particles, and lead to unpredictable particle aggregation following the formation of disulfide bonds as a result. This hypothesis is confirmed by the dramatic effect of DL-dithiothreitol (DTT) on the particle mean diameter (Table 1). DTT is an agent that can reduce the typical disulfide bond via two sequential thiol–disulfide exchange reactions [44]. After adding DTT, the mean diameter of CS–TGA NPs is significantly reduced from 252.3 to 113.0 nm, while that of the CS NPs remains constant (from 240.1 to 245.9 nm). The EE% also decreases with DTT, which indicates what the formation of the disulfide bond favors drug entrapment by thiolated NPs. The surface charge of the NPs is (as expected) positive under these experimental conditions. The zeta-potential of the CS–TGA NPs is twofold lower than that of the CS NPs, due to the presence of thiol groups. The positive surface charge of the CS-based NPs is due to the amino groups [45]. Since the thiol side chains are covalently attached to this primary amino group, it appeares that the existence of thiol side chains in the CS–TGA reduces the charge density by half. It is unaffected by DTT.

Scanning electron microscopy and transmission electron microscopy imaging confirm the morphology and size data of the CS and CS–TGA NPs (Figure 2) [46]. These NPs exhibit a spherical shape with a diameter ranging from 100 to 500 nm.

In vitro release study

Recently, TFV-containing HEC gel was developed as a bioadhesive vaginal drug-delivery system that appears safe and effective in preventing HIV infection [47]. In this study, TFV-loaded HEC gel is used for comparison with the CS and CS–TGA NPs with respect to the drug-release profiles. The drug-release profiles are shown in Figure 3. Approximately 84 and 95% of the cumulative amounts of TFV are released from the HEC gel within 24 and 48 h, respectively. In the case of the CS and CS–TGA NPs, the percentage cumulative release of TFV is 13 and 31% in 24 h and 19 and 39% within 48 h, respectively, and remains constant up to 198 h. These results indicated that the drug-release rate is much faster from the HEC gel. The controlled release of TFV is clearly observed in the case of both the CS and CS–TGA NPs.

In order to predict and correlate the release behavior of the CS and CS–TGA NPs, it is necessary to fit the release data into a suitable mathematical model. The results of curve fitting of drug-release kinetics into different mathematical models are given in Supplementary Figure S3. The zero-order rate describes the systems where the drug-release rate is independent of the concentration of the drug. In the first-order release systems, the drug-release rate is concentration dependent. Higuchi's model describes the release of drugs from an insoluble matrix as a square root of a time-dependent process based on Fickian diffusion [48]. The release constant is calculated from the slope of the appropriate plots, and the r^2 is determined. It was found that the *in vitro* drug release of the CS NPs is best explained by a first-order model, which is the dominant extended-release profile found in hydrophilic matrix systems, as the plots show the highest linearity ($r^2 = 0.990$). The release rate is drug concentration gradient driven. This result is consistent with a previous report related to the the release of tea catechins from CS NPs [45]. The drug release from CS–TGA NPs fits well into Higuchi's equation, as the plots show the highest coefficient of determination ($r^2 = 0.967$) [49]. The insoluble matrix is generated by the disulfide bonds that exist only in CS–TGA NPs in this study. The interdisulfide matrix could prevent the TFV molecules from escaping out of the particles and further decrease the release rate of TFV. The average daily release of TFV is 12% from the CS NPs and 14% from the CS–TGA NPs. As the drug loading of the two kinds of particles are 0.51 (w/w) and 1.62% (w/w) (Table 1), approximately 0.6×10^{-3} and 2.6×10^{-3} mg of drug could be released from 1 mg of CS and CS–TGA NPs every day, respectively. Women of reproductive age produce fluid at a rate of approximately 6 ml/day [50]; the half maximal effective concentration value for TFV is approximately 5 μM [51]. Therefore, approximately 14.6 mg of the CS NPs or 3.9 mg of the CS–TGA NPs would be able to provide the daily requirement of TFV for an adult woman patient, which is feasible considering that the average vaginal suppository, which could be measured as an additional vehicle, had a weight of 5 g.

Cytotoxicity studies

An ideal vaginal drug-delivery system should have no impact on the viability, function and structural integrity of the vaginal epithelium. The selected vaginal epithelial cell line VK2/E6E7 and human endocervical epithelial cell line End1/E6E7 are used to test the effects of NPs on cell membrane integrity and cell viability. The LDH membrane integrity assay is a fluorometric assay that is used to measure the release of LDH from cells with a disrupted membrane [52]. After 48 h, the extent of LDH release from the cells incubated with NPs is no more than 10% higher than that of media (Figure 4). The CS and CS–TGA NPs, and native or free TFV caused a nonsignificant release of LDH. MTS is a tetrazolium compound that is bioreduced by viable cells into formazan. The amount of formazan produced is proportional to the number of living cells [53]. The cell viability test provided results that are consistent with the LDH assay, except for the fact that the native TFV led to a 17% reduction in cell viability of the VK2/E6E7 cell line after 48 h of incubation. However, the observed reduction with the native drug is not significant in cells treated by TFV-loaded NPs, suggesting an additional benefit of the nanocarrier (reducing the microbicide local cytotoxicity).

In both assays, although the results vary slightly due to the acceptable and commonly observed experimental errors (e.g., difference in cell counts in different wells [53]), no statistical difference is observed by the Student's *t*-test between the media control and NPs, which indicates the likely noncytotoxic nature of the CS and CS–TGA NPs. Therefore, both the CS and CS–TGA NPs can be regarded as noncytotoxic for vaginal cell lines after 48 h. However, these assays are short-term studies. The long-term effect of the NPs to the vaginal cell lines and vaginal tissue remains to be elucidated in future work.

The vagina has natural flora; the natural flora protects other microorganisms from growing in the vagina and causing infections. When the natural flora is disturbed, infection can set in and cause an unpleasant odor. The microbicide formulations should not disturb the normal vaginal flora. *L. crispatus* is a predominant, normal, vaginal floral species [54]. It is used here as a model bacteria since it can produce hydrogen peroxide and lactic acid, which could maintain the low-pH environment and provide a natural barrier for HIV transmission [27]. No statistical difference is observed between the media control and the NP treatments after incubation for 48 h (Figure 4). These results suggest that neither the CS NP, nor the CS–TGA NPs are harmful to *L. crispatus* within 48 h.

Triton X-100 could dissolve the lipid on the cell membrane and increase the membrane permeability, leading to cell death. After treatment for 48 h, the bacteria incubated with the NPs, native or free TFV, and media appeared to be intact rod-like structures, which is the same as the previously reported morphology of *L. crispatus* [55]. However, the integrity of bacteria incubated with Triton X-100 is destroyed. This result indicates that both the CS and the CS–TGA NPs are harmless to *L. crispatus* within 48 h.

Cellular uptake mechanism study

Particles labeled with fluorescent dyes are frequently used to study cellular uptake quantitatively using a microplate reader and flow cytometry. Based on an earlier study, the

reaction between the isothiocyanate groups of FITC and the amino groups of CS forms a stable covalent bond [20]. Little FITC could leach out from the NPs over 48 h under *in vitro* conditions. Therefore, the intracellular fluorescence cannot be due to the uptake of free dye that is released or dissociated from the NPs. Figures 5A & 5B show the percentage of the CS and CS–TGA NPs taken up by VK2/E6E7 and End1/E6E7 cell lines, respectively. It is evident that more particles are engulfed by cells with a longer incubation period, due to extended exposure. The CS NPs show similar properties and behaviors to the CS–TGA NPs in both cell lines.

The quantification of the percentage of cells uptaking FITC-loaded NPs is investigated using flow cytometry. The fluorescence intensity curves of the cells treated by FITC-loaded NPs are shown in Figures 5C–5H. The cell number is on the y-axis, while the x-axis depicts fluorescence intensity, which indicates the number of particles internalized by the cells. The shifting of the peak to the right along the x-axis means an intensity increase with increasing concentration of FITC-labeled NPs. In the VK/E6E7 cell line, the percentage of FITC-positive cells is 90.1% for the CS NPs and 99.3% for the CS–TGA NPs. In the End1/E6E7 cell line, the values are 92.6 and 98.6% for the CS and CS–TGA NPs, respectively. A significant uptake of NPs is observed in both cell lines treated with different NPs compared with the control. The results confirm that these NPs are successfully internalized into the vaginal cells.

The uptake is confirmed by fluorescence microscopy. Figure 6 shows the localization of NPs in cells. The cell membrane is observed by phase-contrast microscopy. A blue fluorescence dye, bisBenzimide H 33342 trihydrochloride (Sigma-Aldrich), is used to stain the nucleus. It can bind to the minor groove of DNA and impart a blue color to identify the nucleus. The fluorescence signal of FITC-labeled NPs in the cells is detected by the FITC filter. A total of 48 h after incubation, a high level of uptake of FITC-labeled NPs by both VK2/E6E7 and End1/E6E7 cells is observed by fluorescence microscopy (Figure 6).

Inhibition of cellular uptake study

The result of uptake inhibition is shown in Figure 7. The cell viability after treatment with the inhibitors is shown in Supplementary figure S4. The inhibitors do not reduce the cell viability. Cytochalasin D is an actin filament modifier that can inhibit actin polymerization [56]. Cytochalasin D leads to 15% reduced internalization of CS–TGA NPs in the End1/E6E7 cell line, indicating that cytoskeleton reorganization may be a route of the CS–TGA NP uptake by the End1/E6E7 cell line, and actin microfilaments contribute significantly in the End1/E6E7 cell line. Indeed, actin microfilaments are identified in epithelial rat uterine cells [57]. Actin is the driving force for substance uptake, which decreased in the absence of the actin filaments. Macropinocytosis is dependent on the actin assembly on the cell membrane [58,59]. During macropinocytosis, the rims of the membrane fold, extending from the surface, and fuse back with the plasma membrane, which is called membrane ruffling [60]. Cytochalasin D induces depolymerization of the actin filaments formed and, as a result, inhibits the membrane ruffling. However, this entrance mechanism is excluded in this study since phorbolmyristate acetate, a macropinocytosis stimulator, did not increase particle internalization in any cell line, indicating that macropinocytosis is not involved in

NP uptake. An actin assembly-dependent entrance mechanism excluding macropinocytosis is involved in the uptake of the CS–TGA NPs in the End1/E6E7 cell line. Chloropromazine inhibits clathrin-mediated permeation by disrupting the assembly–disassembly of clathrin [61]. The clathrin pathway is also known as 'receptor-mediated endocytosis'. Particles entering the cell via the clathrin pathway are believed to attach to the plasma membrane by specific binding to the receptor, and then a coated pit (a specialized region of the membrane that is coated with clathrin) is formed [62]. Treatment with chlorpromazine does not reduce the uptake of NPs significantly because there is no specific ligand present on the surface of these NPs that can interact with the receptors. Under genistein treatment, a 51 and 35% reduction of the CS and CS–TGA NPs in the VK2/E6E7 cell line, respectively, and a 31 and 30% reduction of the CS and CS–TGA NPs in the End1/E6E7 cell line, respectively, are observed. These reductions are statistically significant compared with the control. Genistein results in the greatest reductions in both cell lines. Caveolae are a specialized type of lipid raft, which is a flask-shaped invagination in the plasma membrane [63]. The caveolae-associated proteins, such as caveolin-1 and caveolin-2, are expressed in a wide type of human cells, including epithelial cells [64]. Genistein is an inhibitor of caveolin-dependent endocytosis, which is used to block lipid raft-mediated endocytosis. In caveolae-mediated internalization, NPs interact through nonspecific charge interactions with the cell. Since both the CS and CS–TGA NPs are positively charged, the cationic charge on the particle surface promotes their electrostatic interaction with the negatively charged cell surface, leading to an enhanced cellular uptake via the caveolin pathway, which is receptor independent [65]. It has been previously reported that the particle size also contributes to the internalization pathways. Particles with a diameter under 200 nm enter cells preferentially via clathrin-mediated endocytosis; particles with a diameter over 200 nm are more likely to go through caveolin-mediated endocytosis [66]. The mean diameters of both the CS and CS–TGA NPs are above 200 nm. This could be another reason why the caveolae-mediated pathway favors these NPs. It is also consistent with a previous report that poly(lactic-*co*-glycolic) acid NPs with a mean diameter over 200 nm are primarily internalized via the same pathway [9]. Indeed, the internalized caveolae fuse with caveosomes, which could deliver their contents into other subcellular compartments. In comparison with clathrin-dependent endocytosis, the caveolae internalization pathway could avoid acidic and harmful milieu [67]. In summary, caveolin-dependent endocytosis is the most productive route for uptake of these NPs on both cell lines, while cytoskeleton reorganization, which only occurs within the End1/E6E7 cell lines for reasons currently not understood, also contributes as a minor fraction to the uptake mechanism. A similar result has been reported using the CS–DNA complex in HT1080 cells [68]. However, since none of these inhibitors completely eliminate particle uptake, it is evident that other internalization pathways are involved. The same NPs could be internalized via different pathways. For example, it remains to be known if megalin (an endocytic receptor in reproductive tissue for sex hormone-binding globulin) also acts as a pathway for the uptake of these NPs [69].

Bioadhesion studies

The mucus layer covering the epithelia could protect the epithelia against mechanical and chemical damage. It consists mainly of glycoprotein chains with cysteine-rich subdomains [70]. The enhanced mucoadhesive properties of thiomers, such as CS–TGA, are believed to

be based on an interaction of thiolated groups of polymers with the cysteine-rich subdomains of mucus glycoprotein. The evidence of these disulfide bridge formations has been provided in previous literature [15,71].

Porcine vaginal tissue shows a high level of similarity to human vaginal tissue in not only ultrastructural organization and lipid composition, but also secretions in terms of pH and inflammatory responses [72]. These similarities in structure and function have led to the use of porcine tissue as a promising experimental tissue model in studies of the vaginal drug-delivery system. Preliminary study demonstrates that the mucosal tissue remains viable 3 h after death [73]. No significant difference has been shown in the histological structure or water permeability of the mucosal tissue snap-frozen in liquid nitrogen in comparison with fresh tissue [74].

Figure 8 shows the mucoadhesion of the CS and CS–TGA NPs. According to Figure 8A, the mucoadhesive property of the CS–TGA NPs is four- to five-fold higher in comparison with that of the unmodified CS NPs, which is consistent with a previous report [75]. The percentage of mucoadhesion of lower concentration CS–TGA NPs increased considerably when the incubation time was prolonged, as shown in Figure 8B. The formation of disulfide bonds between the CS–TGA NPs and the mucus gel layer is based on a crosslinking process via the thiol/disulfide exchange reactions or a simple oxidation process of free thiol groups [14]. By delaying the reaction time, more disulfide bonds can be formed from oxidation of the thiol groups. Hence, the mucoadhesion adhered covalently on the surface of the mucus layer. However, the increase of the percentage of mucoadhesion of higher concentration NPs (3 mg/ml) is not statistically significant compared with that of the lower concentration NPs (1 mg/ml); perhaps due to the limited number of reactive groups on the tissue surface. The maximum percentage of bioadhesion was 65% (± 3%) with the 200-nm-sized NP for a 2-h duration. The data indicates that mucoadhesion is a time- and concentration-dependent process.

Figure 8C demonstrates the tissue sections visualized using fluorescence microscopy. The tissue treated with the CS NPs shows a very weak fluorescence, while a strong intensity is observed from the tissue treated with fluorescently labeled CS–TGA NPs. The FITC label efficiency of the CS–TGA is 1.5-times that of CS (data not shown). However, it is obvious that the amount of CS–TGA NPs adhered on the surface of the vaginal tissue is much greater than that of the CS NPs on the tissue.

Conclusion

In this work, it is reported for the first time that anti-HIV microbicide (TFV)-loaded, thiolated CS NPs can be a highly mucoadhesive (65%) and noncytotoxic vaginal drug-delivery system. The *in vitro* drug release, cytotoxicity assay and mucoadhesion studies suggest that CS–TGA NPs have the potential to be a controlled-release, safe and bioadhesive microbicide-delivery system. These properties make thiolated CS NPs a good candidate for a topical vaginal microbicide-delivery system for further study related to the quest for new methods for the prevention of HIV transmission.

Future perspective

Mucoadhesive drug-delivery systems are designed to extend the retention time of the drug at the site of application, as well as to provide a controlled release rate of the drug. Most of the commercially available vaginal dosage forms (e.g., vaginal gels) cause a somewhat uncomfortable wetness and leakage. The application of NPs to the vagina may be beneficial to patients by causing much less discomfort and, simultaneously, reducing the frequency of administration. However, further in-depth studies of this drug-delivery system are needed. What is the effectiveness of the antiviral activity of the NPs? What is the retention time of the NPs in the body of animals? What is the longer-term effect of the NPs to vaginal tissue? There are numerous questions that need to be answered.

Supplementary Material

Refer to Web version on PubMed Central for supplementary material.

References

Papers of special note have been highlighted as:

▪ of interest

▪▪ of considerable interest

1. Hackley, VA.; Ferraris, CF. NIST Recommended Practice Guide. National Institute of Standards and Technology; Washington DC, USA: 2001. The Use of Nomenclature in Dispersion Science and Technology.
2. UNAIDS. Global Report UNAIDS Report on the Global AIDS Epidemic 2013. UNAIDS; Geneva, Switzerland: 2013. Introduction; p. 4-11.
3. Krishnan S, Dunbar MS, Minnis AM, Medlin CA, Gerdts CE, Padian NS. Poverty, gender inequities, and women's risk of human immunodeficiency virus/AIDS. Ann NY Acad Sci. 2008; 1136:101–110. [PubMed: 17954681]
4. UNAIDS. Global Report UNAIDS Report on the Global AIDS Epidemic 2013. UNAIDS; Geneva, Switzerland: 2013. Eliminate gender inequalities and gender-based abuse and violence and increase thecapacity of women and girls to protect themselves from HIV; p. 78-83.
5. Askew I, Berer M. The contribution of sexual and reproductive health services to the fight against HIV/AIDS: a review. Reprod Health Matt. 2003; 11(22):51–73.
6. Weber J, Desai K, Darbyshire J. The development of vaginal microbicides for the prevention of HIV transmission. PLoS Med. 2005; 2(5):e142. [PubMed: 15916473]
7. Ndesendo VM, Pillay V, Choonara YE, Buchmann E, Bayever DN, Meyer LC. A review of current intravaginal drug delivery approaches employed for the prophylaxis of HIV/AIDS and prevention of sexually transmitted infections. AAPS PharmSciTech. 2008; 9(2):505–520. [PubMed: 18431651]
8▪. Mamo T, Moseman EA, Kolishetti N, et al. Emerging nanotechnology approaches for HIV/AIDS treatment and prevention. Nanomedicine (Lond). 2010; 5(2):269–285. Discusses the advantages of polymer-based nanoparticles (NPs). [PubMed: 20148638]
9▪. Zhang T, Sturgis TF, Youan BB. pH-responsive nanoparticles releasing tenofovir intended for the prevention of HIV transmission. Eur J Pharm Biopharm. 2011; 79(3):526–536. Shows that pH-sensitive NPs and chitosan–thioglycolic acid-conjugated NPs have many common features. [PubMed: 21736940]
10. Alukda D, Sturgis T, Youan BB. Formulation of tenofovir-loaded functionalized solid lipid nanoparticles intended for HIV prevention. J Pharm Sci. 2011; 100(8):3345–3356. [PubMed: 21437910]

11. Sosnik A. Nanotechnology contributions to the pharmacotherapy of pediatric HIV: a dual scientific and ethical challenge and a still pending agenda. Nanomedicine (Lond). 2010; 5(6):833–837. [PubMed: 20735219]
12. Murugeshu A, Astete C, Leonardi C, Morgan T, Sabliov CM. Chitosan/PLGA particles for controlled release of alpha-tocopherol in the GI tract via oral administration. Nanomedicine (Lond). 2011; 6(9):1513–1528. [PubMed: 21707297]
13. Roldo M, Hornof M, Caliceti P, Bernkop-Schnurch A. Mucoadhesive thiolated chitosans as platforms for oral controlled drug delivery: synthesis and in vitro evaluation. Eur J Pharm Biopharm. 2004; 57(1):115–121. [PubMed: 14729087]
14▪▪. Bernkop-Schnurch A. Thiomers: a new generation of mucoadhesive polymers. Adv Drug Deliv Rev. 2005; 57(11):1569–1582. Defines the thiomers, analyzes different approaches to obtain thiomers and, finally, discusses the application of thiomers. [PubMed: 16176846]
15. Leitner VM, Walker GF, Bernkop-Schnurch A. Thiolated polymers: evidence for the formation of disulphide bonds with mucus glycoproteins. Eur J Pharm Biopharm. 2003; 56(2):207–214. [PubMed: 12957634]
16. Meng J, Sturgis TF, Youan BB. Engineering tenofovir loaded chitosan nanoparticles to maximize microbicide mucoadhesion. Eur J Pharm Sci. 2011; 44(1–2):57–67. [PubMed: 21704704]
17. Grim SA, Romanelli F. Tenofovir disoproxil fumarate. Ann Pharmacother. 2003; 37(6):849–859. [PubMed: 12773076]
18. Jang KI, Lee HG. Stability of chitosan nanoparticles for L-ascorbic acid during heat treatment in aqueous solution. J Agric Food Chem. 2008; 56(6):1936–1941. [PubMed: 18284198]
19. Fernandez-Urrusuno R, Calvo P, Remunan-Lopez C, Vila-Jato JL, Alonso MJ. Enhancement of nasal absorption of insulin using chitosan nanoparticles. Pharm Res. 1999; 16(10):1576–1581. [PubMed: 10554100]
20. Thongborisute J, Takeuchi H, Yamamoto H, Kawashima Y. Visualization of the penetrative and mucoadhesive properties of chitosan and chitosan-coated liposomes through the rat intestine. J Liposome Res. 2006; 16(2):127–141. [PubMed: 16753967]
21. Ma Z, Lim LY. Uptake of chitosan and associated insulin in Caco-2 cell monolayers: a comparison between chitosan molecules and chitosan nanoparticles. Pharm Res. 2003; 20(11):1812–1819. [PubMed: 14661926]
22. Kätzel U, Vorbau M, Stintz M, Gottschalk-Gaudig T, Barthel H. Dynamic light scattering for the characterization of polydisperse fractal systems: II. Relation between structure and DLS results. Part Syst Charact. 2008; 25:19–30.
23. Sassi AB, Isaacs CE, Moncla BJ, Gupta P, Hillier SL, Rohan LC. Effects of physiological fluids on physical–chemical characteristics and activity of topical vaginal microbicide products. J Pharm Sci. 2008; 97(8):3123–3139. [PubMed: 17922539]
24. Don TM, Hsu SH, Chiu WY. Structures and thermal properties of chitosan-modified poly(methyl methacrylate). J Polym Sci. 2001; 39:1646–1655.
25. Nayak AK, Laha B, Sen KK. Development of hydroxyapatite-ciprofloxacin bone-implants using ‘quality by design’. Acta Pharm. 2011; 61(1):25–36. [PubMed: 21406341]
26. Lackman-Smith C, Osterling C, Luckenbaugh K, et al. Development of a comprehensive human immunodeficiency virus type 1 screening algorithm for discovery and preclinical testing of topical microbicides. Antimicrob Agents Chemother. 2008; 52(5):1768–1781. [PubMed: 18316528]
27. Jorgenson, JH.; Turnidge, JD.; Washington, JA., et al. Antibacterial susceptibility tests: dilution and disk diffusion methods. In: Murray, PR.; Baron, EJ.; Pfaller, MA.; Tenover, FC.; Yolken, RH., editors. Manual of Clinical Microbiology (Seventh Edition). ASM Press; Washington DC, USA: 1999. p. 1327-1341.
28. Xie J, Wang CH. Self-assembled biodegradable nanoparticles developed by direct dialysis for the delivery of paclitaxel. Pharm Res. 2005; 22(12):2079–2090. [PubMed: 16132339]
29. Pifer MA, Kibuule LK, Maerz T, Studzinski DM, Baker KC, Herkowitz HN. *In vitro* response of human chondrocytes to a combination of growth factors and a proteinase inhibitor. Orthopedics. 2012; 35(1):35–42. [PubMed: 22229919]
30▪. Douglas KL, Piccirillo CA, Tabrizian M. Cell line-dependent internalization pathways and intracellular trafficking determine transfection efficiency of nanoparticle vectors. Eur J Pharm

Biopharm. 2008; 68(3):676–687. Describes a method for cellular uptake study. [PubMed: 17945472]

31. Ranga Rao KV, Buri P. A novel *in situ* method to test polymers and coated microparticles for bioadhesion. Endocr Rev. 1989; 52 15(13):265–270.
32. Albrecht K, Zirm EJ, Palmberger TF, Schlocker W, Bernkop-Schnurch A. Preparation of thiomer microparticles and *in vitro* evaluation of parameters influencing their mucoadhesive properties. Drug Dev Ind Pharm. 2006; 32(10):1149–1157. [PubMed: 17090437]
33. Grabovac V, Guggi D, Bernkop-Schnurch A. Comparison of the mucoadhesive properties of various polymers. Adv Drug Deliv Rev. 2005; 57(11):1713–1723. [PubMed: 16183163]
34▪. Dudhania A, Kosaraju S. Bioadhesive chitosan nanoparticles: preparation and characterization. Carbohyd Polym. 2010; 81:243–251. Discusses a method for the study of mucoadhesion.
35. Lopes LB, Ferreira DA, De Paula D, et al. Reverse hexagonal phase nanodispersion of monoolein and oleic acid for topical delivery of peptides: *in vitro* and *in vivo* skin penetration of cyclosporin A. Pharm Res. 2006; 23(6):1332–1342. [PubMed: 16715364]
36. Montgomery, D. Design and Analysis of Experiments. John Wiley and Sons Inc; NY, USA: 1995. Response surface methods and design; p. 405-458.
37. Ferreira SL, Bruns RE, Da Silva EG, et al. Statistical designs and response surface techniques for the optimization of chromatographic systems. J Chromatogr A. 2007; 1158(1–2):2–14. [PubMed: 17416377]
38. Vander Heyden Y, Nijhuis A, Smeyers-Verbeke J, Vandeginste BG, Massart DL. Guidance for robustness/ruggedness tests in method validation. J Pharm Biomed Anal. 2001; 24(5–6):723–753. [PubMed: 11248467]
39. Miller, JN.; Miller, JC. Statistics and Chemometrics for Analytical Chemistry. 5. Pearson Education; NJ, USA: 2010. Significance tests; p. 39-69.
40. Bei D, Marszalek J, Youan BB. Formulation of dacarbazine-loaded cubosomes – part II: influence of process parameters. AAPS PharmSciTech. 2009; 10(3):1040–1047. [PubMed: 19688599]
41. Nagarwal RC, Singh PN, Kant S, Maiti P, Pandit JK. Chitosan nanoparticles of 5-fluorouracil for ophthalmic delivery: characterization, *in-vitro* and *in-vivo* study. Chem Pharm Bull (Tokyo). 2011; 59(2):272–278. [PubMed: 21297311]
42. Choi SU, Bui T, Ho RJ. pH-dependent interactions of indinavir and lipids in nanoparticles and their ability to entrap a solute. J Pharm Sci. 2008; 97(2):931–943. [PubMed: 17546665]
43. Van Gelder J, Witvrouw M, Pannecouque C, et al. Evaluation of the potential of ion pair formation to improve the oral absorption of two potent antiviral compounds, AMD3100 and PMPA. Int J Pharm. 1999; 186(2):127–136. [PubMed: 10486430]
44. Cleland WW. Dithiothreitol, a new protective reagent for Sh groups. Biochemistry. 1964; 3:480–482. [PubMed: 14192894]
45. Hu B, Pan C, Sun Y, Hou Z, Ye H, Zeng X. Optimization of fabrication parameters to produce chitosan-tripolyphosphate nanoparticles for delivery of tea catechins. J Agric Food Chem. 2008; 56(16):7451–7458. [PubMed: 18627163]
46. Nasti A, Zaki NM, De Leonardis P, et al. Chitosan/TPP and chitosan/TPP-hyaluronic acid nanoparticles: systematic optimisation of the preparative process and preliminary biological evaluation. Pharm Res. 2009; 26(8):1918–1930. [PubMed: 19507009]
47. Abdool Karim Q, Abdool Karim SS, Frohlich JA, et al. Effectiveness and safety of tenofovir gel, an antiretroviral microbicide, for the prevention of HIV infection in women. Science. 2010; 329(5996):1168–1174. [PubMed: 20643915]
48▪▪. Costa P, Sousa Lobo JM. Modeling and comparison of dissolution profiles. Eur J Pharm Sci. 2001; 13(2):123–133. Discusses the models and equations of drug release/dissolution from solid pharmaceutical dosage forms. [PubMed: 11297896]
49. Merchant HA, Shoaib HM, Tazeen J, Yousuf R. Once-daily tablet formulation and *in vitro* release evaluation of cefpodoxime using hydroxypropyl methylcellulose: a technical note. AAPS PharmSciTech. 2006; 7(3):78. [PubMed: 17025258]
50. Baloglu E, Senyigit ZA, Karavana SY, Bernkop-Schnurch A. Strategies to prolong the intravaginal residence time of drug delivery systems. J Pharm Sci. 2009; 12(3):312–336.

51. Lee WA, He GX, Eisenberg E, et al. Selective intracellular activation of a novel prodrug of the human immunodeficiency virus reverse transcriptase inhibitor tenofovir leads to preferential distribution and accumulation in lymphatic tissue. Antimicrob Agents Chemother. 2005; 49(5): 1898–1906. [PubMed: 15855512]
52. Uboldi C, Bonacchi D, Lorenzi G, et al. Gold nanoparticles induce cytotoxicity in the alveolar type-II cell lines A549 and NCIH441. Part Fibre Toxicol. 2009; 6:18. [PubMed: 19545423]
53. Au C, Mutkus L, Dobson A, Riffle J, Lalli J, Aschner M. Effects of nanoparticles on the adhesion and cell viability on astrocytes. Biol Trace Elem Res. 2007; 120(1–3):248–256. [PubMed: 17916977]
54. Wilks M, Wiggins R, Whiley A, et al. production of vaginal Identification and H_2O_2 lactobacilli from pregnant women at high risk of preterm birth and relation with outcome. J Clin Microbiol. 2004; 42(2):713–717. [PubMed: 14766841]
55. Verhelst R, Verstraelen H, Claeys G, et al. Comparison between Gram stain and culture for the characterization of vaginal microflora: definition of a distinct grade that resembles grade I microflora and revised categorization of grade I microflora. BMC Microbiol. 2005; 5:61. [PubMed: 16225680]
56. Casella JF, Flanagan MD, Lin S. Cytochalasin D inhibits actin polymerization and induces depolymerization of actin filaments formed during platelet shape change. Nature. 1981; 293(5830):302–305. [PubMed: 7196996]
57. Luxford KA, Murphy CR. Cytoskeletal control of the apical surface transformation of rat uterine epithelium. Biol Cell. 1993; 79(2):111–116. [PubMed: 8161965]
58. Meng H, Yang S, Li Z, et al. Aspect ratio determines the quantity of mesoporous silica nanoparticle uptake by a small GTPase-dependent macropinocytosis mechanism. ACS Nano. 2011; 5(6):4434–4447. [PubMed: 21563770]
59. Mercer J, Helenius A. Virus entry by macropinocytosis. Nat Cell Biol. 2009; 11(5):510–520. [PubMed: 19404330]
60. Perumal, Op; Inapagolla, R.; Kannan, S.; Kannan, RM. The effect of surface functionality on cellular trafficking of dendrimers. Biomaterials. 2008; 29(24–25):3469–3476. [PubMed: 18501424]
61. Pho MT, Ashok A, Atwood WJ. JC virus enters human glial cells by clathrin-dependent receptor-mediated endocytosis. J Virol. 2000; 74(5):2288–2292. [PubMed: 10666259]
62. Benmerah A, Lamaze C. Clathrin-coated pits: vive la difference? Traffic. 2007; 8(8):970–982. [PubMed: 17547704]
63▪. Manes S, Del Real G, Martinez AC. Pathogens: raft hijackers. Nat Rev Immunol. 2003; 3(7):557–568. Demonstrates the mechanism of caveolin-mediated internalization. [PubMed: 12876558]
64. Rybin VO, Grabham PW, Elouardighi H, Steinberg SF. Caveolae-associated proteins in cardiomyocytes: caveolin-2 expression and interactions with caveolin-3. Am J Physiol Heart Circ Physiol. 2003; 285(1):H325–H332. [PubMed: 12649076]
65. Georgieva JV, Kalicharan D, Couraud PO, et al. Surface characteristics of nanoparticles determine their intracellular fate in and processing by human blood–brain barrier endothelial cells *in vitro*. Mol Ther. 2011; 19(2):318–325. [PubMed: 21045812]
66. Rejman J, Oberle V, Zuhorn IS, Hoekstra D. Size-dependent internalization of particles via the pathways of clathrin- and caveolae-mediated endocytosis. Biochem J. 2004; 377(Pt 1):159–169. [PubMed: 14505488]
67. Bathori G, Cervenak L, Karadi I. Caveolae – an alternative endocytotic pathway for targeted drug delivery. Crit Rev Ther Drug Carrier Syst. 2004; 21(2):67–95. [PubMed: 15202927]
68. Peng SF, Tseng MT, Ho YC, Wei MC, Liao ZX, Sung HW. Mechanisms of cellular uptake and intracellular trafficking with chitosan/DNA/poly(gamma-glutamic acid) complexes as a gene delivery vector. Biomaterials. 2011; 32(1):239–248. [PubMed: 20864162]
69▪. Hammes A, Andreassen TK, Spoelgen R, et al. Role of endocytosis in cellular uptake of sex steroids. Cell. 2005; 122(5):751–762. Provides various endocytosis pathways for cellular uptake of NPs. [PubMed: 16143106]
70. Dekker J, Rossen JW, Buller HA, Einerhand AW. The MUC family: an obituary. Trends Biochem Sci. 2002; 27(3):126–131. [PubMed: 11893509]

71. Bernkop-Schnurch A, Schwarz V, Steininger S. Polymers with thiol groups: a new generation of mucoadhesive polymers? Pharm Res. 1999; 16(6):876–881. [PubMed: 10397608]

72. Squier CA, Mantz MJ, Schlievert PM, Davis CC. Porcine vagina *ex vivo* as a model for studying permeability and pathogenesis in mucosa. J Pharm Sci. 2008; 97(1):9–21. [PubMed: 17721937]

73. Nicolazzo JA, Reed BL, Finnin BC. The effect of various *in vitro* conditions on the permeability characteristics of the buccal mucosa. J Pharm Sci. 2003; 92(12):2399–2410. [PubMed: 14603485]

74. Lesch CA, Squier CA, Cruchley A, Williams DM, Speight P. The permeability of human oral mucosa and skin to water. J Dent Res. 1989; 68(9):1345–1349. [PubMed: 2476469]

75. Bernkop-Schnurch A, Hornof M, Guggi D. Thiolated chitosans. Eur J Pharm Biopharm. 2004; 57(1):9–17. [PubMed: 14729077]

Executive summary

Nature of nanomedicine

- The anti-HIV microbicide-loaded chitosan(CS)–thioglycolic acid-conjugated nanoparticles (NPs) are prepared by ionotropic gelation. The NPs tested are spherical, with diameters ranging from 240 to 252 nm. They provide a controlled release of the drug following the Higuchi model, while the control hydroxyethylcellulose gel exhibited bursts and immediate drug release.

Nanotoxicology

- The CS–thioglycolic acid-conjugated NPs are not cytotoxic to either vaginal epithelial cell lines or *Lactobacillus* over 48 h.

NP uptake mechanism

- The cellular uptake is time dependent. It mainly occurrs via caveolin-mediated endocytosis.

NP mucoadhesion

- The mucoadhesive property of CS–thioglycolic acid-conjugated NPs is fivefold higher than that of CS NPs.

Conclusion and future perspective

- CS–thioglycolic acid-conjugated NPs are a promising nanomedicine template for topical microbicide delivery in the vagina.

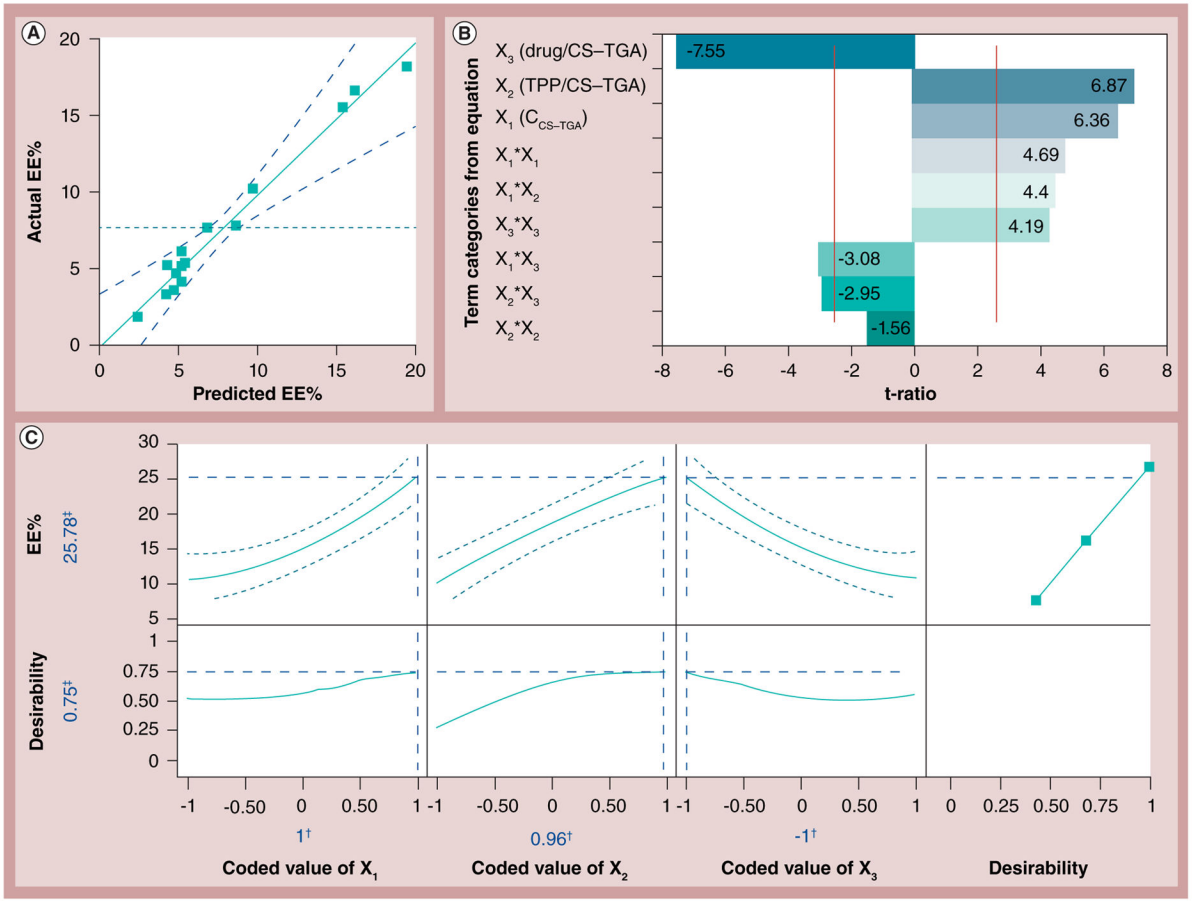

Figure 1. Outputs of the encapsulation efficiency optimization process using Box–Behnken design

(A) Curve fitting of EE%, where the coefficient of determination = 0.98. The solid line represents the regression line surrounded by dashed curvilinear boundaries showing the 95% confidence data distribution limit. The horizontal dashed line represents the mean of the actual EE% value. **(B)** Standardized Pareto chart showing the standardized effect of the formulation variables and their interaction with EE%. X-axis indicates the t-ratios of the variables and the y-axis shows the categories of terms. The two vertical lines indicate the positive and negative $t_{Critical}$ values and reach statistical significance ($\alpha = 0.05$). The values indicated on the bars represent the standardized effects, which are the t-values calculated based on Equation 11. **(C)** Prediction profiler showing the effect of the formulation variables on EE% surrounded by dashed curviliear boundaries showing the 95% confidence data distribution limit (± 3.77%).

†Optimal positions of X values.

‡Optimal position of Y values.

CS–TGA: Concentration of chitosan–thioglycolic acid conjugate; EE%: Encapsulation efficiency; TPP: Sodium tripolyphosphate; X_1: Concentration of chitosan–thioglycolic acid conjugate (w/v%); X_2: Sodium tripolyphosphate/chitosan–thioglycolic acid conjugate weight ratio; X_3: Drug/chitosan–thioglycolic acid conjugate weight ratio.

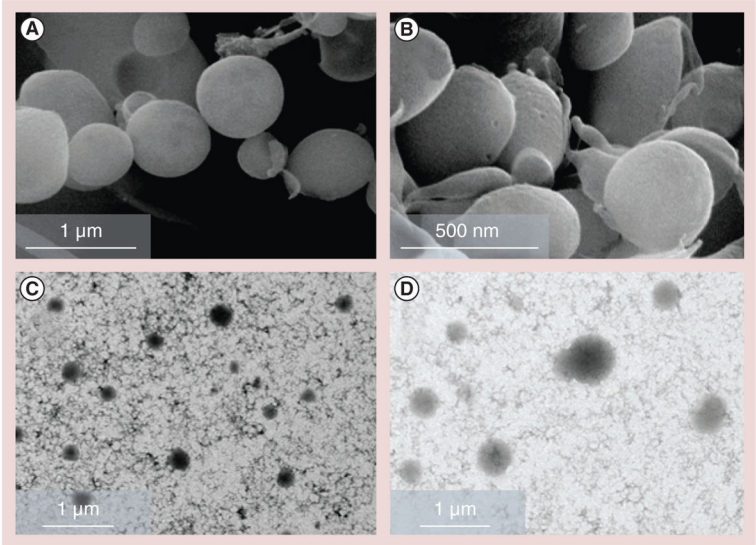

Figure 2. Morphological analysis of the nanoparticles

Scanning electron microscopy images of **(A)** chitosan (CS) nanoparticles (NPs) and **(B)** CS–thioglycolic acid conjugate NPs, and transmission electron microscopy images of **(C)** CS NPs and **(D)** CS–thioglycolic acid conjugate NPs. All of the four images are obtained with samples prepared with a concentration of chitosan–thioglycolic acid conjugate (w/v%) of 1, a sodium tripolyphosphate/chitosan–thioglycolic acid conjugate weight ratio of 0.96 and a drug/chitosan–thioglycolic acid conjugate weight ratio of −1.

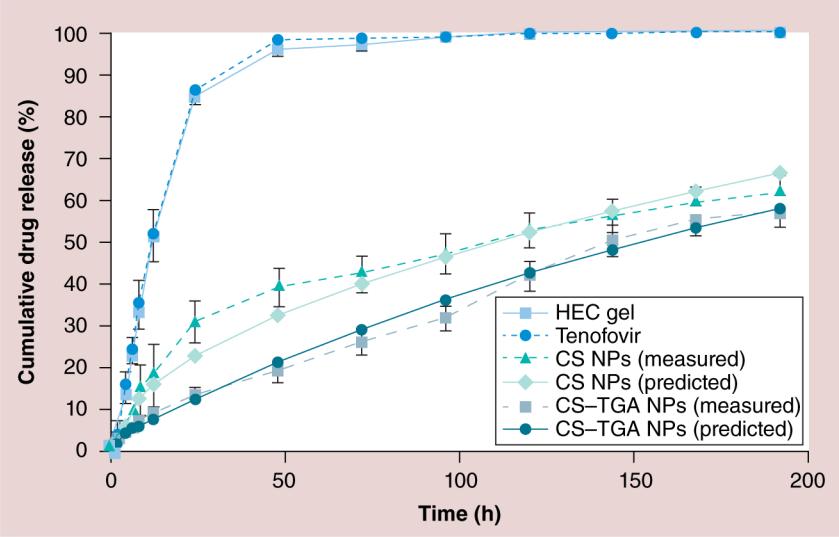

Figure 3. *In vitro* drug-release profiles from chitosan and chitosan–thioglycolic acid conjugate nanoparticles, in vaginal fluid stimulant (pH of 4.2; n = 3)

Both samples are prepared with a concentration of CS–TGA (w/v%) of 1, a sodium tripolyphosphate/CS–TGA weight ratio of 0.96 and a drug/CS–TGA weight ratio of −1. Data are shown as mean ± the standard error of the mean (n = 3).

CS: Chitosan; CS–TGA: Chitosan–thioglycolic acid conjugate; HEC: Hydroxyethyl cellulose; NP: Nanoparticle.

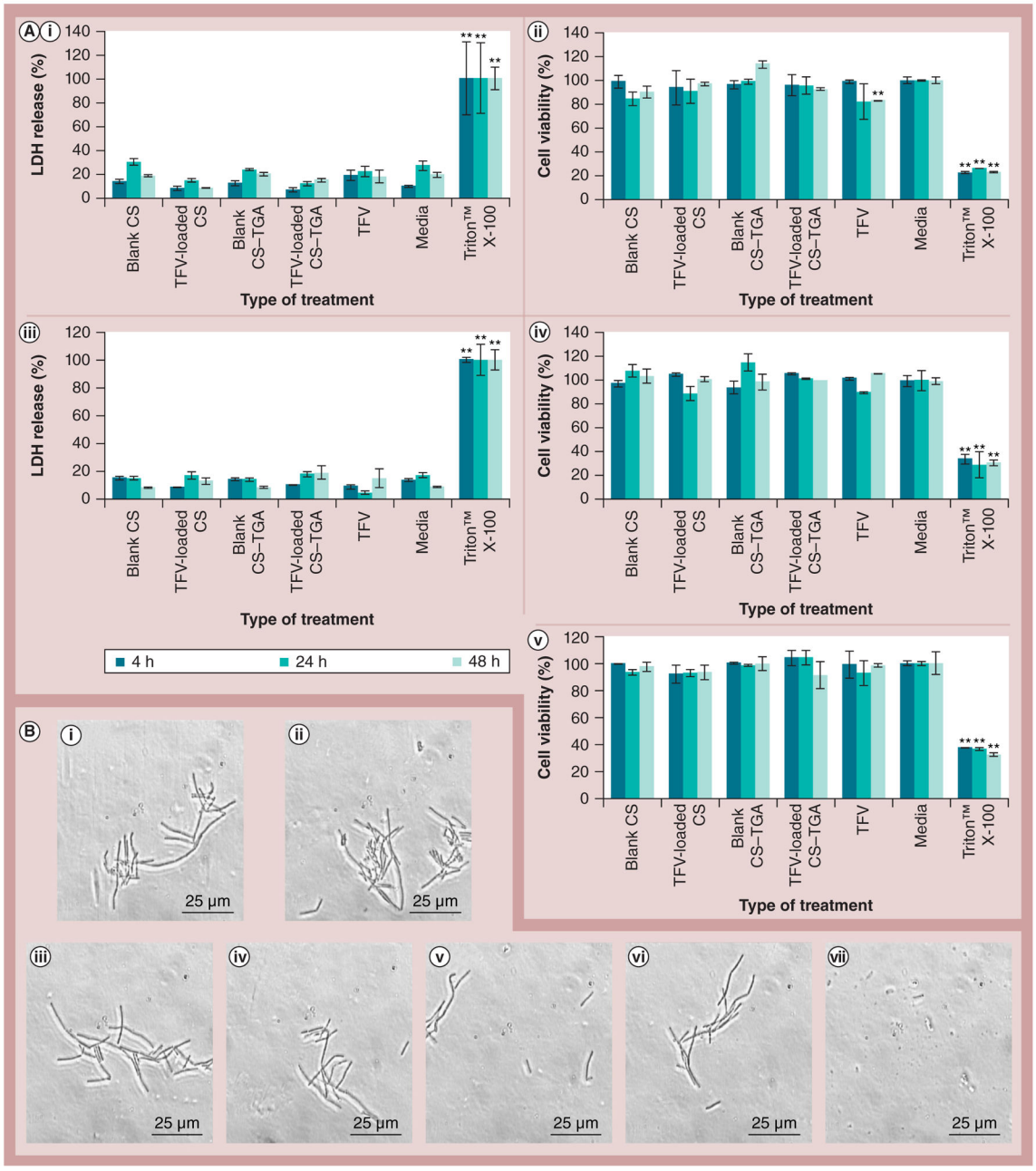

Figure 4. Cytotoxicity study of tenofovir-loaded chitosan and chitosan–thioglycolic acid conjugate nanoparticles

(A) Percentage LDH release of **(A,i)** VK2/E6E7 cell line and **(A,iii)** End1/E6E7 cell line. Percentage viability of **(A,ii)** VK2/E6E7 cell line and **(A,iv)** End1/E6E7 cell line and **(A,v)** *Lactobacillus crispatus*. **(B)** *L. crispatus* morphologies under microscopy after incubation with **(B,i)** blank CS nanoparticles (NPs), **(B,ii)** TFV-loaded CS NPs, **(B,iii)** blank CS–TGA NPs, **(B,iv)** TFV-loaded CS–TGA NPs, **(B,v)** free TFV (see detailed NPs characteristics in Table 2), **(B,vi)** media and **(B,vii)** Triton™ X-100 (Sigma-Aldrich, MO, USA). Cells are incubated with the NPs for 48 h. Data are shown as mean ± the standard error of the mean (n = 3).

**$p < 0.01$ vs media.

CS: Chitosan; CS–TGA: Chitosan–thioglycolic acid conjugate; LDH: Lactate dehydrogenase; TFV: Tenofovir.

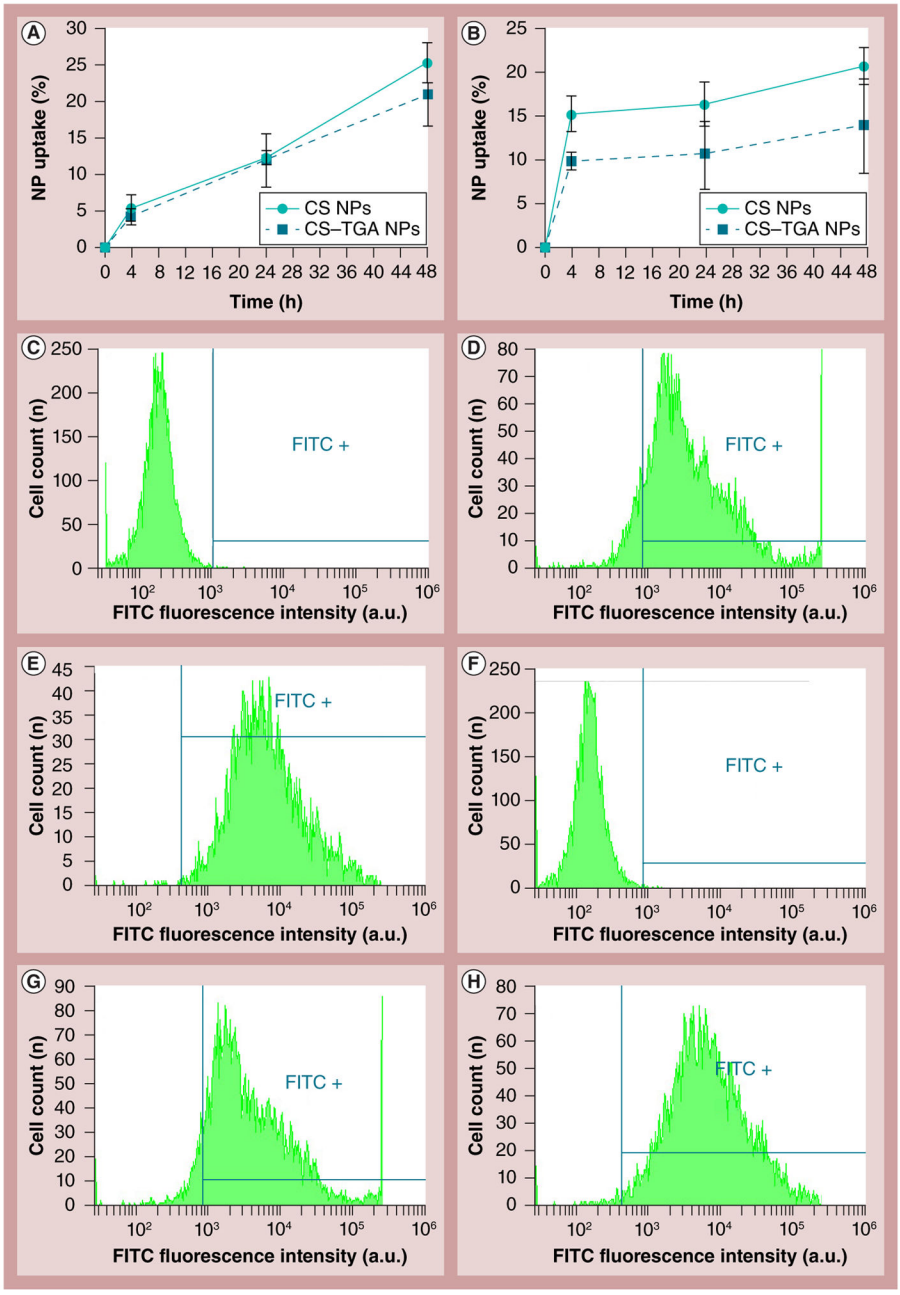

Figure 5. Cellular uptake study by fluorometry assays

The particle uptake efficiency of FITC-labeled CS and CS–TGA NPs on **(A)** the VK2/E6E7 cell line and **(B)** the End1/E6E7 cell line. Cells are incubated with NPs for 48 h. Data are shown as mean ± the standard error of the mean (n = 3). NP cellular uptake is assessed by flow cytometry (cell count vs FITC fluorescence intensity) in: VK2/E6E7 cell line treated with **(C)** cell culture media alone as control, **(D)** FITC-labeled CS NPs and **(E)** FITC-labeled CS–TGA NPs; End1/E6E7 cell line treated with **(F)** cell culture media alone as control, **(G)** FITC-labeled CS NPs and **(H)** FITC-labeled CS–TGA NPs for 48 h. NPs are prepared with a concentration of chitosan–thioglycolic acid conjugate (w/v%) of 1, a sodium

tripolyphosphate/chitosan–thioglycolic acid conjugate weight ratio of 0.96 and a drug/chitosan–thioglycolic acid conjugate weight ratio of −1. In parts (C–H) the area labeled FITC+ shows the fluorophore signal in the cell with a detectable level of FITC. The horizontal and vertical lines are the boundary of the FITC positive area.
a.u.: Arbitrary unit; CS: Chitosan; CS–TGA: Chitosan–thioglycolic acid conjugate; FITC: Fluorescein isothiocyanate; NP: Nanoparticle.

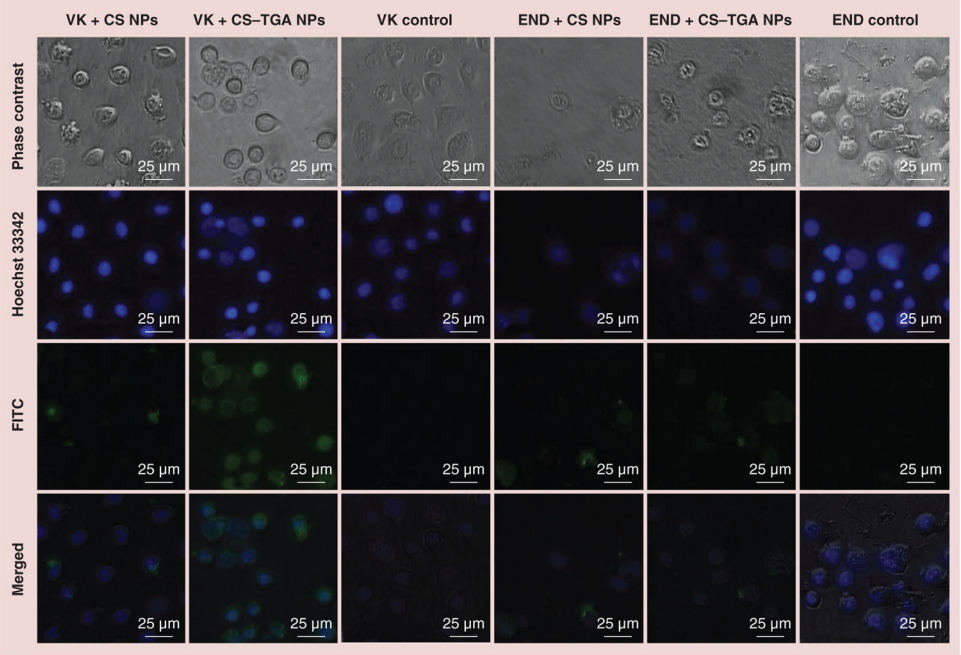

Figure 6. *In vitro* localization of fluorescein isothiocyanate-labeled chitosan- and chitosan–thioglycolic acid-conjugated nanoparticles in VK2/E6E7 and End1/E6E7 cell lines by fluorescence microscopy

Cells are observed under phase contrast microscopy, and Hoechst 33342 (excitation: 330–380 nm; emission: 420 nm) and FITC (excitation: 490–500 nm; emission: 535 nm) fluorescence filter sets (Nikon, Tokyo, Japan) are used to observe the nucleus (blue) and the NPs (green), respectively. The three images are then merged.

CS: Chitosan; CS–TGA: Chitosan–thioglycolic acid conjugate; END: End1/E6E7 cell line; Hoechst 33342: BisBenzimide H 33342 trihydrochloride (Sigma-Aldrich, MO, USA); FITC: Fluorescein isothiocyanate; NP: Nanoparticle; VK: VK2/E6E7 cell line.

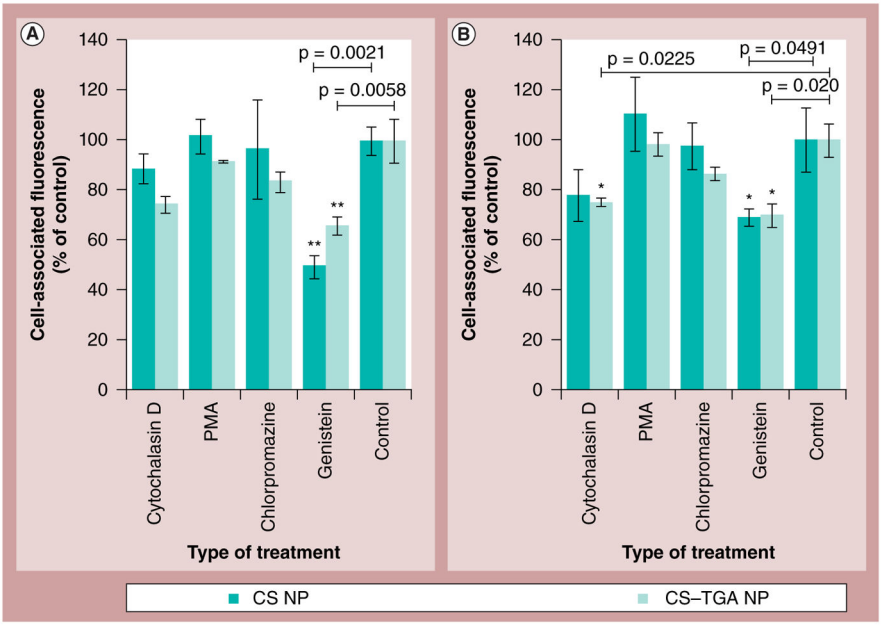

Figure 7. Results of uptake mechanism studies

Effects of inhibitors on uptake of fluorescein isothiocyanate-labeled nanoparticles on **(A)** the VK2/E6E7 cell line and **(B)** the End1/E6E7 cell line. Cells are incubated with nanoparticles for 24 h and lysed by 1% Triton™ X-100 (Sigma-Aldrich, MO, USA). Nanoparticles are prepared with a concentration of chitosan–thioglycolic acid conjugate (w/v%) of 1, a sodium tripolyphosphate/chitosan–thioglycolic acid conjugate weight ratio of 0.96 and a drug/chitosan–thioglycolic acid conjugate weight ratio of −1. Data are shown as the mean ± the standard error of the mean (n = 3).

*$p < 0.05$ verus control.

**$p < 0.01$ versus control.

PMA: Phorbolmyristate acetate.

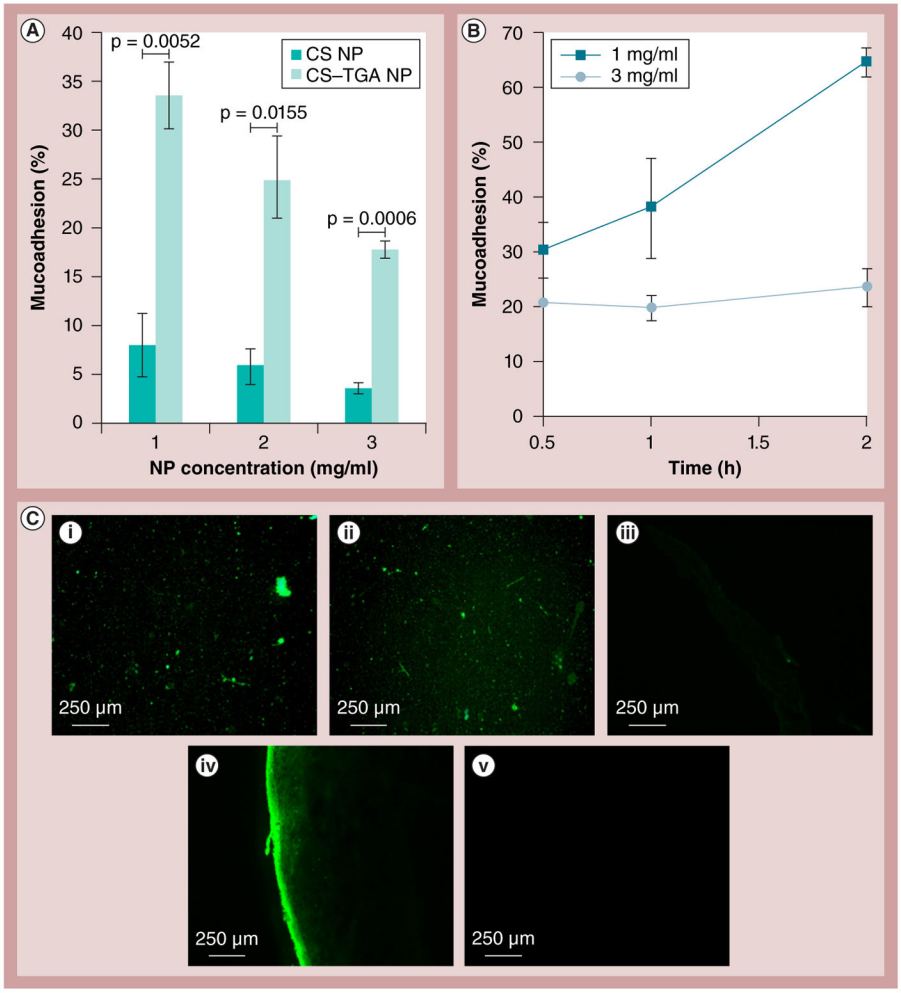

Figure 8. Results of the nanoparticle mucoadhesion studies

(A) Concentration-dependent percentage mucoadhesion by infusion method; and **(B)** time-dependent percentage mucoadhesion by immersion method. **(C,i)** Fluorescence microcopy of fluorescein isothiocyanate-CS NPs suspension (3 mg/ml) and **(C,ii)** fluorescein isothiocyanate-CS–TGA NPs suspension (3 mg/ml). Thin sections of porcine vaginal tissue treated with **(C,iii)** suspension A, **(C,iv)** suspension B and **(C,v)** media. NPs are prepared with a concentration of CS–TGA conjugate (w/v%) of 1, a sodium tripolyphosphate/chitosan–thioglycolic acid conjugate weight ratio of 0.96 and a drug/chitosan–thioglycolic acid conjugate weight ratio of −1. Data are shown as mean ± the standard error of the mean (n = 3). CS: Chitosan ; CS–TGA: Chitosan–thioglycolic acid conjugate; NP: Nanoparticle.

Table 1

Effect of DL-dithiothreitol on the size, zeta-potential and encapsulation efficiency of chitosan-and chitosan–thioglycolic acid-conjugated nanoparticles.

NPs	Mean diameter (nm)	PDI	Zeta-potential (mV)	EE%	Drug loading (w/w%)
CS	240.1 ± 3.3	0.298 ± 0.002	43.9 ± 0.6	5.4 ± 1.0	0.51 ± 0.09
CS + DTT	245.9 ± 28.1	0.212 ± 0.029	44.4 ± 5.4	6.5 ± 0.6	0.61 ± 0.06
CS–TGA	252.3 ± 16.3	0.317 ± 0.052	21.4 ± 2.4	19.4 ± 1.1	1.6 ± 0.11
CS–TGA ± DTT	113.0 ± 7.5**	0.305 ± 0.020	20.2 ± 3.2	6.5 ± 1.4**	0.61 ± 0.13

Data are given as mean ± SEM for n = 3.

** $p < 0.01$.

CS: Chitosan; CS–TGA: Chitosan–thioglycolic acid conjugate; DTT: DL-dithiothreitol; EE%: Encapsulation efficiency; NP: Nanoparticle; PDI: Polydispersity index.

Table 2

Checkpoint experiments comparing measured and predicted encapsulation efficiencies (n=3).

Run (n)	X_1	X_2	X_3	Measured Y_1 ± SEM (%)	Predicted Y_1	Error of (%) Y_1	p-value (Y_1)	t-value (Y_1)
C1	−0.5	−0.5	−0.5	3.90 ± 1.01	4.81	−18.09	0.46	0.90
C2	0.5	0.5	0.5	6.79 ± 0.80	7.37	−7.87	0.54	0.72
C3	1	0.96	−1	22.60 ± 1.06	25.78	−12.34	0.10	3.00

SEM: Standard error of the mean; X_1: Concentration of chitosan–thioglycolic acid conjugate (w/v%); X_2: Sodium tripolyphosphate/chitosan–thioglycolic acid conjugate weight ratio; X_3: Drug/chitosan–thioglycolic acid conjugate weight ratio; Y_1: Encapsulation efficiency.